Pre-Print Manuscript of Article:
Bridgelall, R., "Connected Vehicle Approach for Pavement Roughness Evaluation," *Journal of Infrastructure Systems*, American Society of Civil Engineering, 20(1), pp. 1-6, 2014.

A Connected Vehicle approach for pavement roughness evaluation

Raj Bridgelall, Ph.D.[1]

Abstract

Connected vehicles present an opportunity to monitor pavement condition continuously by analyzing data from vehicle-integrated position sensors and accelerometers. The current practice of characterizing and reporting ride-quality is to compute the international roughness index (IRI) from elevation profile or bumpiness measurements. However, the IRI is defined only for a reference speed of 80 kilometers per hour. Furthermore, the relatively high cost for calibrated instruments and specialized expertise needed to produce the IRI limit its potential for widespread use in a connected vehicle environment. This research introduces the road impact factor (RIF) which is derived from vehicle integrated accelerometer data. The analysis demonstrates that RIF and IRI are directly proportional. Simultaneous data collection with a laser-based inertial profiler validates this relationship. A linear combination of the RIF from different speed bands produces a time-wavelength-intensity-transform (TWIT) that, unlike the IRI, is wavelength-unbiased. Consequently, the TWIT enables low-cost, network-wide and repeatable performance measures at any speed. It can extend models that currently use IRI data by calibrating them with a constant of proportionality.

[1]Program Director and Assistant Professor of Transportation, Upper Great Plains Transportation Institute, North Dakota State University, P.O. Box 863676, Plano, TX 75086. Phone: 408-607-3214, E-mail: raj@bridgelall.com

CE Database subject headings: Forecasting; Frequency response; Information technology (IT); Intelligent transportation systems; Maintenance costs; Pavement management; Preservation; Probe instruments; Remote sensing; Surface roughness

Author Keywords: Ride quality; Performance measures; Connected Vehicle

Introduction

The international roughness index (IRI) and power spectral density (PSD) are the two indices most widely used to summarize ride-quality and pavement condition. Producing them requires calibrated profiling equipment and personnel with specialized training. Even with the latest high-speed profiling technologies, transportation agencies cannot afford the time and expense necessary to produce ride-quality measures more frequently than once per year. Consequently, symptoms of distress conditions go unnoticed. An example is a frost heave that appears and disappears in between data collection cycles. To mitigate these problems, agencies are seeking lower-cost approaches to comply with federal condition reporting requirements for the national highway network.

The IRI is derived from the accumulated suspension movement of a simulated quarter-car called the Golden Car, rolling over an elevation profile at a fixed reference speed of 80 kilometers per hour (km/h), which is about 50 miles per hour (Gillespie 1981). The IRI is undefined at other speeds, making it nearly impossible to characterize ride-quality for urban roads using the existing standard. The mechanical filter model used to compute IRI emphasizes wavelength energy near the modal resonances, and attenuates those that fall outside of the frequency pass-band. This filtering action results in wavelength biases that could mask some distress symptoms (Marcondes et al. 1991). Consequently, practitioners often utilize the PSD to detect underlying or developing faults by analyzing the full, unbiased wavelength composition of

an elevation profile. Computing the PSD requires sample sequences from relatively long pavement sections, thereby limiting its use for distress symptom localizing within a few meters of the actual problem area (Perera and Kohn 2005).

The IRI is currently the recommended means of quantifying ride-quality. Even though its shortcomings are widely acknowledged, no other research has demonstrated an improved means or lower cost methods to produce it. Several efforts examined the possibility of estimating the IRI or the elevation profile from accelerometer data but have not derived a theoretical relationship. A research team from the University of Tokyo found that the root-mean-square (RMS) of the accelerometer signal was correlated to the elevation profile data (Fujino et al. 2005). A team from the University of Pretoria (South Africa) found that it is possible to train an artificial neural network to estimate the elevation profile from accelerometer data, within 20% accuracy (Ngwangwa et al. 2010). An Auburn University team recently produced similar results by training an artificial neural network to estimate the IRI. They found that the RMS of the accelerometer output generally provided a better correlation with the IRI (Dawkins et al. 2011).

This research derived improved indices, the road impact factor (RIF) and its corresponding time-wavelength-intensity-transform (TWIT). They combine the localization capabilities of the IRI with the broad-band spectral decomposition features of the PSD. Transportation agencies in the United States and other countries are collaborating with leading vehicle manufacturers to promote travel safety and efficiency through vehicle-to-vehicle (V2V) and vehicle-to-infrastructure (V2I) communications (USDOT 2012). When enabled in connected vehicle protocols, centralized computing platforms will access data from vehicle accelerometers and global positioning system (GPS) receivers or odometers to produce a ride-quality for any speed. This research derives, simulates, and validates a direct proportionality relationship between the

RIF and the IRI. A linear combination of RIF from a broad range of speeds produces the TWIT, which is also directly proportional to the IRI but is significantly less wavelength-biased. A connected vehicle compatible means of characterizing ride-quality will reduce the cost of pavement condition monitoring and broaden substantially its scope and regularity from existing inspection approaches. The proportionality relationship with IRI can extend existing deterioration forecasting models with data from connected vehicles by directly substituting the IRI for TWIT and a constant of proportionality.

Theoretical framework

The next sections present an analytical framework to examine relationships between the RIF, TWIT and IRI as functions of bump height, bump width, and longitudinal speed.

Bump model

Let the bump function be a continuously differentiable Gaussian radial bases function (Buhmann 2008):

$$z(x) = \alpha \exp\left(-\left[\xi\left(x-\chi\right)\right]^2\right) \tag{1}$$

The amplitude is α, the distance from the origin is χ, and the sharpness is ξ. Let the approximate bump width λ be:

$$\lambda = \frac{\sqrt{2\pi e}}{\xi} \tag{2}$$

where *e* is a mathematical constant that is the base of the natural logarithm. Fig 1(a) shows the spatial elevation profile of a four centimeter high by one meter wide bump *z(x)* as a function of bump width or longitudinal distance *x*, and its second derivative $\ddot{z}(x)$, which is the slope change

profile. The latter is in units of slope/meter and represents the rate of change of slope with respect to longitudinal distance.

The vertical acceleration energy produced from traversing a bump is directly proportional to the slope change profile and the square of the speed σ. This relationship is derived later. The intensity and frequency composition of the vertical acceleration energy increases with longitudinal speed and decreases when bumps are wider. Fig 1(b) shows the Fourier Transform of the vertical acceleration energy produced from traversing a four centimeter high by one-meter wide bump at σ = 8 km/h, the same bump traversed at 12 times the longitudinal speed σ, and a bump that is half as wide (0.5 × w) and traversed at σ = 8 km/h. The overall suspension response of a typical vehicle has the characteristic shape shown in Fig 1(b) where the positions of the lower and upper peaks are the sprung and unsprung mass resonances of the mechanical filter respectively (Jazar 2008). The model for the suspension response spectra in this simulation is a double pole, Type-I Chebyshev band-pass filter with pass-band ripple factor of 2.1. It is implemented as a digital infinite impulse response filter with low and high cutoff frequencies of 1-hertz and 12.5-hertz respectively. The vehicle suspension responds in proportion to the product of the bump spectra and the vehicle response spectra. It is evident that the suspension response in this model will approach a peak for speeds approaching 8 km/h and then taper off as the bump energy translates away from the modal resonance at higher speeds.

The IRI wavelength bias

Defining $U_z(x)$ as a rectified elevation profile (REP), which is an accumulation of the rectified slope $\dot{z}(x)$, gives:

$$U_z(x) = \int_0^x |\dot{z}(\varsigma)| d\varsigma \tag{3}$$

Fig 2 shows the REP relative to an example spatial elevation profile $z(x) = z_1(x) + z_2(x) + z_3(x)$ that consists of three bumps $z_1(x)$, $z_2(x)$ and $z_3(x)$where the parameter matrix for their height α, distance from the origin χ, and approximate width λ in meters are:

$$\begin{bmatrix} \alpha_1 & \chi_1 & \lambda_1 \\ \alpha_2 & \chi_2 & \lambda_2 \\ \alpha_3 & \chi_3 & \lambda_3 \end{bmatrix} = \begin{bmatrix} 0.04 & 0.5 & 1 \\ 0.04/4 & 1.5 & 1/2 \\ 0.04/16 & 2.0 & 1/4 \end{bmatrix} \tag{4}$$

The values are selected so that a bump that is half as wide must also be one quarter shorter to produce an equal intensity slope change profile. Incidentally, a linear combination of bumps with randomly distributed heights, widths, and location simulates a characteristic road elevation profile.

The Golden Car mechanical filter pass-band characteristics are similar to the Chebyshev model previously introduced. Fig 2 compares the magnitude of the suspension stroke accumulations for a Golden Car traversing the three previously defined bumps at a constant speed of 8 km/h and 80 km/h. After traveling 3 meters at a speed of 8 km/h, the accumulated IRI is greater than the REP. Conversely, the accumulated IRI is less than the REP when traveling the same distance at a speed of 80 km/h. As described earlier, traveling at a much higher speed translates the vertical acceleration energy further away from the suspension modal resonance, which leads to significantly less IRI accumulation. Hence, it is not possible to compare bumpiness from IRI accumulated at different speeds.

The road impact factor

The slope rate, which is the second derivative of equation (1), produces the vertical acceleration from traversing a single bump such that:

$$\ddot{z}(t) = \frac{d^2}{dt^2}\left[\alpha \exp\left(-\left[\xi\left(x(t)-\chi\right)\right]^2\right)\right] = \left(2\xi^2\sigma\right)^2\left[\chi^2 - \frac{1}{2\xi^2} - 2\chi\sigma t + \left(\sigma t\right)^2\right]\alpha \exp\left(-\left[\xi\left(\sigma t-\chi\right)\right]^2\right) \quad (5)$$

The temporal elevation profile is $z[x(t)]$. Applying the chain rule of differentiation to the composite function $z[x(t)]$ provides the general solution:

$$\ddot{z}(t) = \frac{d^2}{dt^2} z(x(t)) = \ddot{x}(t)\dot{z}(x) + \dot{x}(t)^2 \ddot{z}(x) \quad (6)$$

For the special case of constant speed where $\dot{x}(t) = \sigma(t) = \sigma$ the longitudinal acceleration is $\ddot{x}(t) = 0$ and the expression simplifies to $\ddot{z}(t) = \sigma^2 \ddot{z}[x]$.

The vertical acceleration response that a vehicle occupant feels is a convolution of the vertical acceleration input with the impulse response of the vehicle suspension filter $v_z(t)$ such that:

$$S_{out}(t) = \int v_z(t-\tau)\ddot{z}(\tau)d\tau \quad (7)$$

An accelerometer mounted to the body of the vehicle measures this vertical acceleration as $g_z(t) = \gamma \times S_{out}(t)$, where γ is the accelerometer proportionality constant. The average vertical acceleration experienced when traveling at a constant speed σ across a portion of the road, which is a road segment of length L is:

$$\overline{g}^L = \frac{1}{L}\int_0^L g_z(x)dx = \frac{1}{L}\int_0^T g_z(t)\sigma(t)dt = \frac{1}{L}\int_0^{L/\overline{\sigma}} g_z(t)\sigma(t)dt \quad (8)$$

because $dx = \sigma(t)dt$. The Parseval Theorem relates the energy of the signal in the temporal and frequency domains (Oppenheim and Schaefer 1975) as:

$$\int \left|G_z(f)\right|^2 df = \int \left|g_z(t)\right|^2 dt \quad (9)$$

Defining the road impact factor (RIF) as:

$$R^L[k] = \sqrt{\frac{1}{L}\int_0^{L/\overline{\sigma}} \left|g_z(t)\sigma(t)\right|^2 dt} \quad (10)$$

essentially utilizes the time domain accelerometer signal to quantify the average vertical acceleration energy produced from segment *k* per unit distance L. Fig 3(a) compares the RIF and the accumulated 'IRI' for a range of speeds across the same 4-centimeter high by 1-meter wide bump. The RIF is a function of the resultant vehicle suspension response sensed at the accelerometer position and the suspension impulse response as defined in equation (7). The IRI quarter-car mechanical filter assumes nearly a factor of two amplification of the sprung mass resonance over the unsprung mass resonance (Gillespie 1981). This amplification difference and a coupling of the spring responses produce the two local maxima observed below the 50 km/h region. The Chebyshev model of the suspension response at the accelerometer location assumes equal responses from both of the modal excitations. Therefore, the RIF response shows a smoother transition as bump energy shifts from lower to higher frequencies. For a fixed longitudinal speed, both RIF and IRI are directly proportional to the bump height as shown in Fig 3(b).

The time-wavelength-intensity-transform

Let the time-wavelength-intensity-transform (TWIT), denoted by the dependent variable Ψ, be the weighted average RIF by traffic volume N within a speed window of size $\Delta\sigma$ such that:

$$\Psi_k(\Delta P_j) = \frac{\sum_{w=1}^{N_k} \overline{R}_{\Delta\sigma_w}^{\Delta P_j}[k] \times N_{\Delta\sigma_w}^{\Delta P_j}[k]}{\sum_{w=1}^{N_k} N_{\Delta\sigma_w}^{\Delta P_j}[k]} \tag{11}$$

The data collection time-interval is ΔP, which could be any resolution desired, for example minutes, hours or days, and ΔP_j is an integer time index j for the analysis. Therefore, the total analysis time elapsed is $\Delta P \times j$. Similarly, the speed window index w contains parameters from traversals where the speed σ falls within the speed range $(w\text{-}1)\times\Delta\sigma < \sigma \le \Delta\sigma \times w$. The average

RIF and the number of vehicles traveling across segment k, within the speed band $\Delta\sigma_w$, and in time increment ΔP_j is $\overline{R}_{\Delta\sigma_w}^{\Delta P_j}[k]$ and $N_{\Delta\sigma_w}^{\Delta P_j}[k]$ respectively. The total number of speed bands available for segment k is N_k. Fig 4(a) is a graphical representation of the TWIT for data taken from a hypothetical road segment, and accumulated for a time-period of one day. It is a histogram of the relative vehicle volume N for each of the $w = \{1 \ldots 8\}$ speed bands that are $\Delta\sigma$ = 5km/h wide. The lower vertical axis is the average RIF computed for data within each of the eight speeds bands.

From Bernoulli's Theorem (Papoulis 1991), as the vehicle volume across the segment grows, the average RIF measured at a given speed will converge to the ride quality that the occupant of a typical vehicle experiences. Therefore, as the number of traversals and speed bands increase, the TWIT produces a less wavelength biased representation of the pavement distress symptoms. The weighted linear combination of RIF creates an adaptive property that emphasizes wavelengths that most significantly affect ride quality at speeds that a majority of users travel the segment.

The vertical acceleration potential

Defining a vertical acceleration potential (VAP) $E_z(L)$ gives:

$$E_z(L) = \sqrt{\frac{1}{L}\int_0^L \left|\ddot{z}(\varsigma)\right|^2 d\varsigma} \tag{12}$$

The VAP is in units of slope per foot of longitudinal distance and is a speed-independent measure of the spatial profile bumpiness. From equation (6), the slope rate, which is the vertical acceleration input to a vehicle traveling a profile $z(x)$ at some speed σ, is directly proportional to

the slope change profile $\ddot{z}(x)$. Equation (12) shows that VAP is an LTI transformation of the slope change profile.

Combining equations (7) and (10) yields:

$$R^L[k] = \sqrt{\frac{1}{L}\int_0^{L/\bar{\sigma}} \left|\sigma(t)\left[\gamma \int v_z(t-\tau)\ddot{z}(\tau)d\tau\right]^2 dt\right|} \tag{13}$$

which shows that RIF is an LTI transformation of the slope rate. From the distributive property of LTI systems (Chen 2004), the RIF, and by extension its linear combination, the TWIT, must be directly proportional to the VAP. The experimental results described later validate this postulation. Fig 4(b) shows the TWIT and the VAP for a range of heights of a one-meter wide bump. Their direct proportionality is evident.

Experiments

The North Dakota Department of Transportation provided test data from an inertial profiler equipped with left wheel path (LWP) and right wheel path (RWP) height sensors, an accelerometer positioned on the floor between the driver and passenger seats, and a GPS receiver. Fig 5 shows data collected from six constant speed traversals of a 150-meter section of the IRI test track located near Monticello, Minnesota. The median wheel path (MWP) data is the average of the LWP and RWP measurements. This is compared with the REP previously defined.

The height sensors measure the vertical distance from the vehicle chassis to the wheel path surface. Hence, the data includes height variations from sprung mass modal excitations that produce chassis bounce. The common practice to stabilize the reference plane is to remove the chassis bounce by computing its displacement by double integration of the accelerometer data. However, electronic noise and unknown initial conditions typically lead to errors that result in

inconsistent measurements (Janoff 1990). The differentiation process to produce the REP from the MWP is essentially a high pass filter that attenuates the sprung mass response near one-hertz. This process effectively removes the sensitivity to reference plane bounce as observed by the repeatability of the REP relative to the MWP in the figure.

Results

Let the percent variability of a data set having values $\{D_1, D_2, \ldots, D_N\}$ be:

$$V = \frac{\frac{1}{N}\sum_{n=1}^{N}\left|D_n - \overline{D}\right|}{\overline{D}} \tag{14}$$

where $\overline{D}$ is the average of N values. Table 1 summarizes the statistics of the data obtained from the six traversals. The last row lists their variability from the mean as a percentage (V%). As expected, the MWP variability is significantly higher than any of the other statistic, primarily due to the Inertial Profiler reference plane bounce. The REP varies less. The VAP is produced from the second derivative of the MWP and listed in percent slope per meter (% slope/m). The VAP varies less than the REP because of the double derivative. Consequently, the VAP is a candidate speed-independent characterization of bumpiness from Inertial Profiling data. The author will explore this potential in future work.

The inertial profiler sampled the elevation profile at fixed distance intervals regulated by the longitudinal speed shown in the second column. The IRI algorithm converted the spatial elevation profile into a temporal elevation profile by assuming a fixed sample period that is equivalent to capturing the profile samples at the IRI reference speed. The IRI shown in the fourth column is in meters per kilometer (m/km). The IRI variation is slightly less than the VAP because the IRI attenuates any variations in elevation profile energy contributions from

wavelengths outside of the quarter-car mechanical filter pass-band. The VAP is unfiltered, except for the inherent anti-alias filtering of the elevation profiler height sensor.

The RIF is listed in 10^{-3} g per meter. Factors in the overall RIF variation include sensor errors, wheel path variations, traversal distance variations, and traversal time variations. Instead of attempting to quantify the source of all error contributions to the RIF, it would be more insightful to lump the total error into an equivalent factor that is of some significance. From equation (10), the RIF variability for an average traversal speed of $\overline{\sigma}$ is proportional to the ratio $\sqrt{\overline{L}}/\overline{T}$, which are variations in the average path distance and the traversal time because:

$$R^L[k] = \sqrt{\frac{\overline{\sigma}^2}{\overline{L}} \int_0^{\overline{L}/\overline{\sigma}} \left|g_z(t)\right|^2 dt} = \sqrt{\frac{\overline{L}^2}{\overline{T}^2} \frac{1}{\overline{L}} \int_0^{\overline{T}} \left|g_z(t)\right|^2 dt} = \sqrt{\frac{\overline{L}}{\overline{T}^2} \int_0^{\overline{T}} \left|g_z(t)\right|^2 dt} \quad (15)$$

With all other factors being equal, approximately 25 centimeter variation in the average traversal distance of 150 meters would produce the RIF variation listed.

The RIF/VAP ratio is within 5% margin of error and validates the direct proportionality relationship postulated earlier. Similarly, the RIF/IRI ratio validates the hypothesis that one can substitute for the other in models by calibration with a constant of proportionality.

Summary and Conclusions

The RIF is a statistical characterization of ride quality that appears suitable for deployment in a connected vehicle environment. It is proportional to the average energy of the vertical acceleration experienced per unit of longitudinal distance when traveling a segment at a specified speed. The TWIT is a linear combination of the average RIF produced at different speeds. The theoretical derivations, simulations, and experimental results demonstrate that the TWIT is directly proportional to the IRI. The TWIT approaches a wavelength-unbiased characterization of bumpiness as vehicle volume, speed spread, and suspension diversity increases. When

incorporated into pavement deterioration models, the TWIT will produce optimum maintenance triggers based on the ride quality that the actual vehicle population experiences when traveling a segment at prevailing speeds. This property is in contrast to the IRI that characterizes ride-quality at a fixed reference speed. The RIF/IRI proportionality for constant speed traversals could extend models that use IRI to compare and forecast ride-quality at a specified speed.

This research also introduced the VAP, which is an inertial profiler reference plane stabilized and speed-independent characterization of bumpiness. It is derived from elevation profile samples recorded at fixed distance intervals. The VAP is a candidate index to characterize pavement bumpiness in urban driving situations where traffic conditions and irregular road geometry make it impossible to maintain a fixed profiling speed. Future research will examine further the relationship between the VAP and the TWIT and their utility in characterizing the bumpiness of urban roads. Extensions of this research will deploy smart phone apps to collect GPS and accelerometer data at different sample rates to examine TWIT performance tradeoff with vehicle volume.

Acknowledgement

This work is based on research supported by the North Dakota Department of Transportation (NDDOT) and the United Stated Department of Transportation (USDOT), Research and Innovative Technology Administration (RITA) under the Rural Transportation Research Initiative.

Notation

The following symbols are used in this paper:

[C] = Golden Car matrix of damping coefficients;

$E_z(L)$ = VAP for road segment of length L;

e	=	mathematical constant equal to 2.71828;
$g_z(t)$	=	g-force output from a vertical acceleration sensor as a function of time t;
$\bar{g}^L$	=	average g-force experienced on segment of length L;
[k]	=	Golden Car matrix of spring rates;
L	=	longitudinal profile (or segment) length;
[m]	=	Golden Car matrix of sprung and unsprung masses;
N_k	=	number of speed bands available for segment k;
$N_{\Delta\sigma_w}[k]$	=	number of vehicles traveling across segment k, within speed band $\Delta\sigma_w$;
$N^{\Delta P_j}[k]$	=	number of vehicles traveling across segment k, within time-period ΔP_j;
ΔP_j	=	time-period increment instance j;
$R^L[k]$	=	RIF for segment k of length L;
$\overline{R}^{\Delta P_j}[k]$	=	average RIF across segment k, within time-period ΔP_j;
$\overline{R}_{\Delta\sigma_w}[k]$	=	average RIF across segment k, within speed band $\Delta\sigma_w$;
T	=	total traversal time for a segment;
V	=	variability in a set of data points;
$v_z(t)$	=	vehicle suspension system impulse response as a function of time t;
$x(t)$	=	longitudinal distance traveled as a function of time t;
y_s	=	sprung mass linear motion;
y_u	=	unsprung mass linear motion;
$z(x)$	=	spatial elevation profile as a function of longitudinal distance x;
$\dot{z}(x)$	=	slope profile as a function of longitudinal distance x;
$\ddot{z}(x)$	=	slope change profile as a function of longitudinal distance x;

$z(t)$	=	temporal elevation profile as a function of time t;
$\ddot{z}(t)$	=	slope rate as a function of time t;
α	=	bump amplitude;
χ	=	bump distance from the origin;
γ	=	accelerometer proportionality constant;
$\Delta\sigma_w$	=	speed band window size and instance w;
λ	=	approximate bump width;
σ	=	constant longitudinal speed;
$\sigma(t)$	=	longitudinal speed as a function of time;
ξ	=	bump sharpness;
$\Psi_k(\Delta P_j)$	=	TWIT for time-period increment instance j;

References

Buhmann, M. D. (2008). *Radial Basis Functions: Theory and Implementations,* Cambridge University Press, MA.

Chen, C.-T. (2004). *Signals and Systems*, 3rd Ed., Oxford University Press, New York, NY.

Dawkins, J., Bevly, D., Powell, B., and Bishop, R. (2011). *Investigation of Pavement Maintenance Applications of Intellidrive*, University of Virginia, VA.

Fujino, Y., Kitagawa, K., Furukawa, T., and Ishii, H. (2005). "Development of Vehicle Intelligent Monitoring System (VIMS)." SPIE, San Diego, CA, 148–157.

Gillespie, T. D. (1981). "Technical Considerations in the Worldwide Standardization of Road Roughness Measurement." *World Bank Technical Report*, Washington, D.C.

Janoff, M. S. (1990). "The Prediction of Pavement Ride Quality from Profile Measurements of Pavement Roughness." *Surface Characteristics of Roadways: International Research and Technologies*, ASTM, Philadelphia, PA, 259-276.

Jazar, R. N. (2008). *Vehicle Dynamics: Theory and Applications.* Springer, New York, NY.

Marcondes, J., Burgess, G. J., Harichandran, R., and Snyder, M. B. (1991). "Spectral Analysis of Highway Pavement Roughness." *Journal of Transportation Engineering,* 117(5), 540–549.

Ngwangwa, H., Heyns, P., Labuschagne, F., and Kululanga, G. (2010). "Reconstruction of road defects and road roughness classification using vehicle responses with artificial neural networks simulation." *Journal of Terramechanics,* 47(2), 97-111.

Oppenheim, A. V., and Schaefer, R. W. (1975). *Digital Signal Processing*. Prentice-Hall, Englewood Cliffs, NJ.

Papoulis, A. (1991). *Probalility, Random Variables, and Stochastic Processes.* McGraw-Hill, New York, NY.

Perera, R. W., and Kohn, S. D. (2005). *Quantification of Smoothness Index Differences Related to Long-Term Pavement Performance Equipment Type*, Federal Highway Administration, Office of Research, Development, and Technology, McLean, VA.

United States Department of Transportation (USDOT) (2012). "Enabling a Secure Environment for Vehicle-to-Vehicle (V2V) and Vehicle-to-Infrastructure (V2I) Transactions." *April 2012 Public Workshop,* ITS Joint Program Office, Research and Innovative Technology Administration (RITA), Washington, DC.

Table 1. Statistics of test path data

Test	Speed (km/h)	MWP (meters)	IRI (m/km)	REP (meters)	VAP (% slope/m)	RIF (10^{-3} g/m)	RIF/VAP	RIF/IRI
1	55.46	0.089	1.59	0.269	2.71	98.26	36.3	61.8
2	55.56	0.157	1.59	0.292	2.67	95.32	35.7	59.9
3	55.54	0.095	1.59	0.275	2.65	87.94	33.2	55.3
4	55.61	0.153	1.54	0.294	2.64	94.99	36.0	61.7
5	55.69	0.217	1.56	0.335	2.75	91.99	33.5	59.0
6	55.79	0.134	1.57	0.286	2.65	98.53	37.2	62.8
AVG	55.61	0.141	1.573	0.292	2.68	94.51	35.29	60.08
V%	0.16%	24.73%	1.06%	5.20%	1.29%	3.20%	3.73%	3.33%

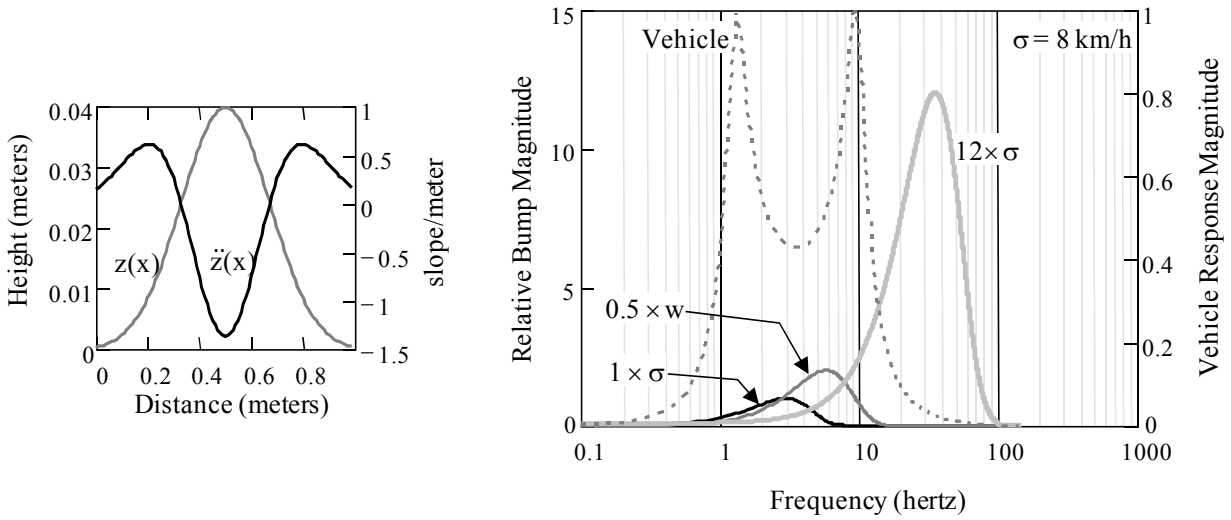

Fig. 1. (a) Bump and slope change profile (b) Frequency spectra of slope rate relative to the vehicle suspension response.

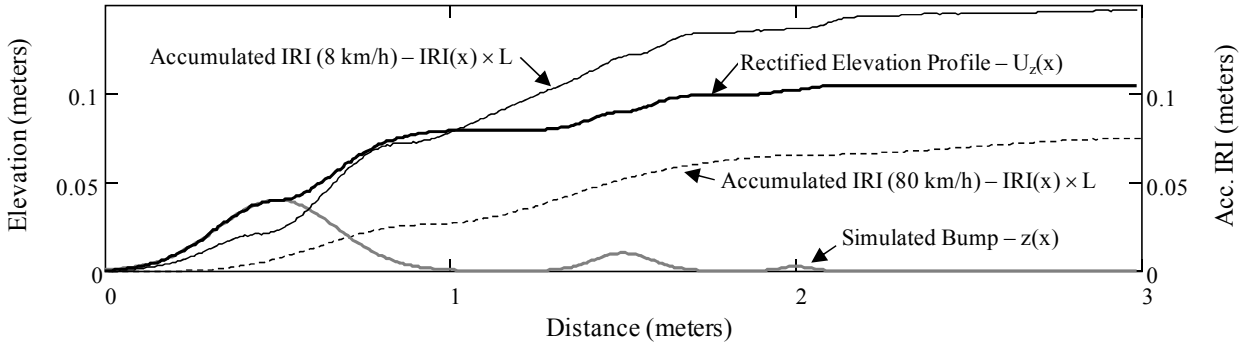

Fig. 2. Simulated bumps, the rectified elevation profile, and IRI accumulations at 8 km/h and 80 km/h.

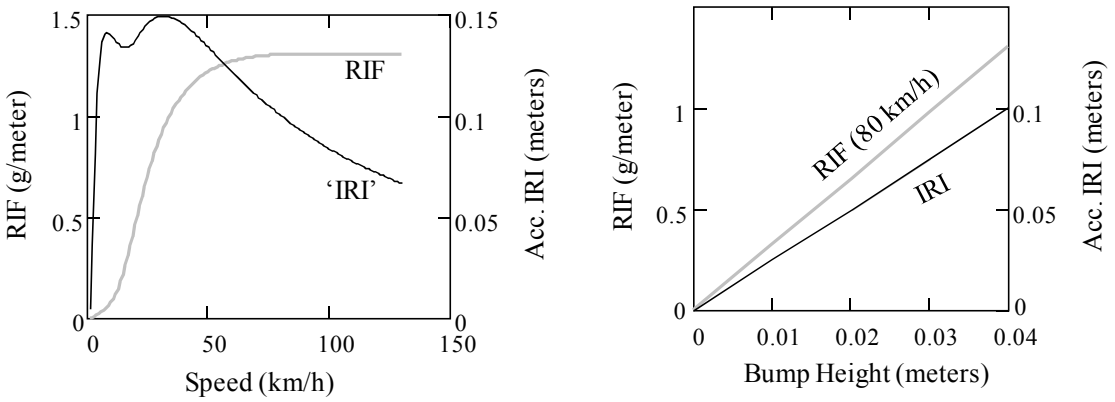

Fig. 3. The RIF and the 'IRI' (a) as a function of speed (b) as a function of bump height at 80 km/h.

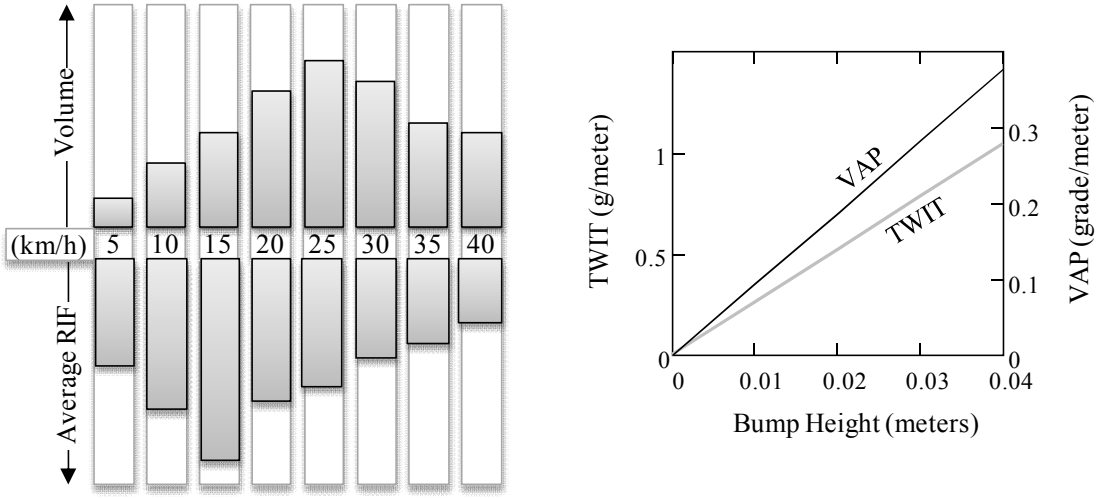

Fig. 4. (a) Graphical representation of the TWIT (b) VAP and TWIT from a 1-meter wide bump.

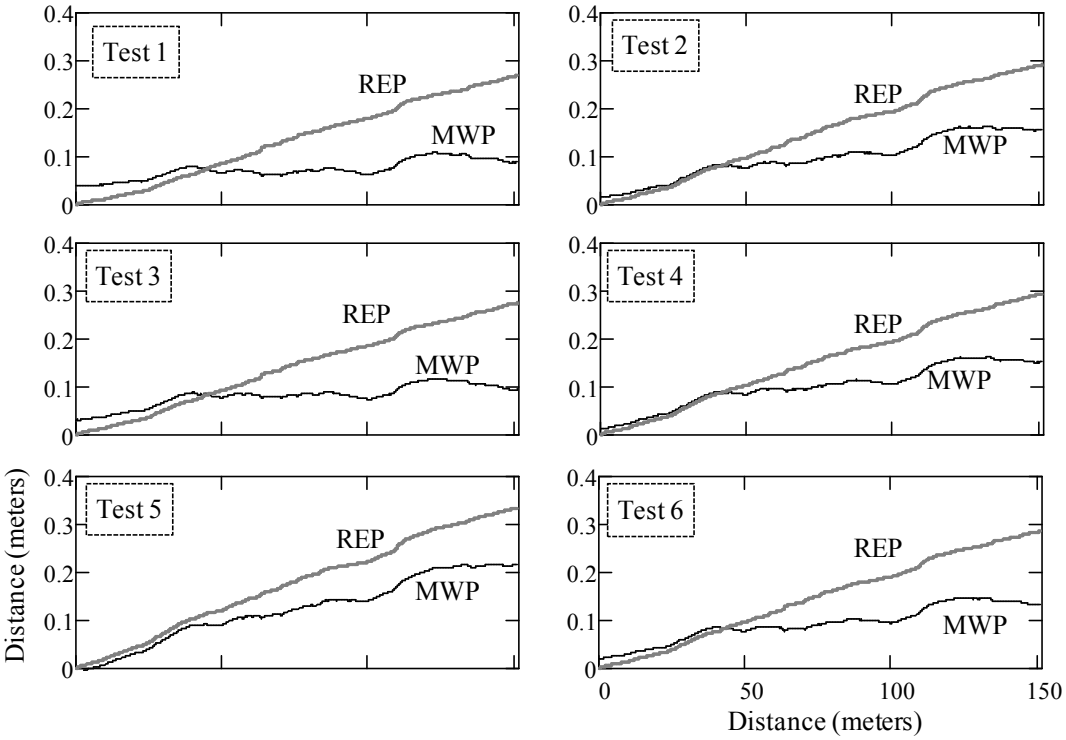

Fig. 5. Inertial Profiler data from multiple test path runs.